

5-9-2018

Methylglyoxal Uptake Coefficients on Aqueous Aerosol Surfaces

David O. De Haan

University of San Diego, ddehaan@sandiego.edu

Natalie G. Jimenez

University of San Diego

Alexia de Loera

University of San Diego

Mathieu Cazaunau

Aline Gratien

See next page for additional authors

Follow this and additional works at: http://digital.sandiego.edu/chemistry_facpub

 Part of the [Physical Chemistry Commons](#)

Digital USD Citation

De Haan, David O.; Jimenez, Natalie G.; de Loera, Alexia; Cazaunau, Mathieu; Gratien, Aline; Pangui, Edouard; and Doussin, Jean-Francois, "Methylglyoxal Uptake Coefficients on Aqueous Aerosol Surfaces" (2018). *Chemistry and Biochemistry Faculty Publications*. 35.

http://digital.sandiego.edu/chemistry_facpub/35

This Article is brought to you for free and open access by the Department of Chemistry and Biochemistry at Digital USD. It has been accepted for inclusion in Chemistry and Biochemistry Faculty Publications by an authorized administrator of Digital USD. For more information, please contact digital@sandiego.edu.

Methylglyoxal Uptake Coefficients on Aqueous Aerosol Surfaces

Abstract

In order to predict the amount of secondary organic aerosol formed by heterogeneous processing of methylglyoxal, uptake coefficients (γ) and estimates of uptake reversibility are needed. Here, uptake coefficients are extracted from chamber studies involving ammonium sulfate and glycine seed aerosol at high relative humidity ($\text{RH} \geq 72\%$). Methylglyoxal uptake coefficients on prereacted glycine aerosol particles had a strong dependence on RH, increasing from $\gamma = 0.4 \times 10^{-3}$ to 5.7×10^{-3} between 72 and 99% RH. Continuous methylglyoxal losses were also observed in the presence of aqueous ammonium sulfate at 95% RH ($\gamma_{\text{AS,wet}} = 3.7 \pm 0.8 \times 10^{-3}$). Methylglyoxal uptake coefficients measured at $\geq 95\%$ RH are larger than those reported for glyoxal on nonacidified, aqueous aerosol surfaces at 90% RH. Slight curvature in first-order uptake plots suggests that methylglyoxal uptake onto aqueous aerosol surfaces is not entirely irreversible after 20 min. Methylglyoxal uptake by cloud droplets was rapid and largely reversible, approaching equilibrium within the 1 min mixing time of the chamber. PTR-MS measurements showed that each cloud event extracted 3 to 8% of aerosol-phase methylglyoxal and returned it to the gas phase, likely by an oligomer hydrolysis mechanism.

Disciplines

Physical Chemistry

Authors

David O. De Haan, Natalie G. Jimenez, Alexia de Loera, Mathieu Cazaunau, Aline Gratien, Edouard Pangui, and Jean-Francois Doussin

13 ABSTRACT: In order to predict the amount of secondary organic aerosol formed by
14 heterogeneous processing of methylglyoxal, uptake coefficients (γ) and estimates of uptake
15 reversibility are needed. Here, uptake coefficients are extracted from chamber studies involving
16 ammonium sulfate and glycine seed aerosol at high relative humidity (RH $\geq 72\%$).
17 Methylglyoxal uptake coefficients on pre-reacted glycine aerosol particles had a strong
18 dependence on RH, increasing from $\gamma = 0.4 \times 10^{-3}$ to 5.7×10^{-3} between 72 and 99% RH.
19 Continuous methylglyoxal losses were also observed in the presence of aqueous ammonium
20 sulfate at 95% RH ($\gamma_{AS,wet} = 3.7 \pm 0.8 \times 10^{-3}$). Methylglyoxal uptake coefficients measured at
21 $\geq 95\%$ RH are larger than those reported for glyoxal on non-acidified, aqueous aerosol surfaces at
22 90% RH. Slight curvature in 1st-order uptake plots suggests that methylglyoxal uptake onto
23 aqueous aerosol surfaces is not entirely irreversible after 20 min. Methylglyoxal uptake by cloud
24 droplets was rapid and largely reversible, approaching equilibrium within the 1 min mixing time
25 of the chamber. PTR-MS measurements showed that each cloud event extracted 3 to 8% of
26 aerosol-phase methylglyoxal and returned it to the gas phase, likely by an oligomer hydrolysis
27 mechanism.

28 1. Introduction

29 Several studies have estimated the global amount of secondary organic aerosol formed from
30 glyoxal and methylglyoxal via aqueous phase processes. These estimates range from 3 – 13
31 TgC/year for glyoxal¹⁻³ and 1.5 – 8 TgC/year for methylglyoxal.²⁻⁴ Because the surface area and
32 water content of clouds is much larger than that of aqueous aerosol particles, SOA production
33 from dicarbonyls is assumed to take place predominantly in clouds.³ These estimates of SOA
34 production represent significant fractions of total SOA loading in some urban areas,⁵ and have
35 stimulated intense interest in the aqueous chemistry responsible for converting volatile carbonyl
36 species into hydrate, oligomer, and acid products that can remain in the condensed phase after
37 the cloud droplet evaporates. In addition, gas-phase reactions with water vapor or water clusters
38 can convert aldehydes to diols,⁶⁻⁹ blue-shifting their absorbance spectra,⁹ lowering their vapor
39 pressure, and making transfer to clouds and aerosol more likely.

40 Unfortunately, aqueous SOA production estimates for aldehydes are quite uncertain, given
41 questions about the reversibility of uptake, the mechanism of uptake (dependent on surface area
42 or ion catalysis),¹⁰ and the magnitude of the uptake coefficient (γ) itself. Glyoxal uptake
43 coefficients measurements have ranged from $\gamma = 1 \times 10^{-3}$ on aqueous droplets¹¹ to a
44 photochemically enhanced uptake of $\gamma = 16 \times 10^{-3}$ on non-hygroscopic ammonium sulfate / fulvic
45 acid aerosol.^{10, 12} Glyoxal uptake coefficients have been found to depend on aerosol acidity,¹³
46 relative humidity,¹³⁻¹⁴ and ionic strength.¹⁵ While the value of Liggio *et al.*¹³ ($\gamma = 2.9 \times 10^{-3}$ on
47 non-acidified aerosol) is most commonly used in modeling studies,^{3, 16-17} high-end values ($\gamma = 16$
48 $\times 10^{-3}$) have been successfully used to model PM_{2.5} levels in Mexico City.⁵

49 For methylglyoxal, the situation is even more uncertain. To our knowledge, methylglyoxal
50 uptake coefficient has been reported only on 55-85% H₂SO₄ solutions.¹⁸ Modeling studies have

51 adopted glyoxal uptake coefficients for methylglyoxal based on chemical similarity,^{3, 5, 16-17} even
52 though the two molecules are very different in important aspects such as surface activities,¹⁹⁻²¹
53 hydration equilibrium constants,²²⁻²³ Henry's law coefficients,²²⁻²⁶ and oligomerization
54 processes.²⁷⁻²⁸ There is a clear need for measurements of methylglyoxal uptake coefficients onto
55 aerosol and droplet surfaces that have atmospheric relevance. In this study, we extract
56 methylglyoxal uptake coefficients from a series of chamber experiments performed on
57 atmospherically relevant inorganic and organic seed aerosol at high relative humidity levels.

58
59

2. Materials and Methods

60 Experimental methods have been described earlier,²⁹ and will be only briefly described here.
61 The CESAM 4.2 m³ temperature-controlled chamber³⁰⁻³¹ uses input flows of humidified or dry
62 purified air to offset sample flows and maintain constant pressure just above ambient levels. The
63 stirred chamber, whose walls are uncoated 304L stainless steel, is pumped down to a few mTorr
64 between each experiment, and cleaned with pure ethanol (VWR, 99%) and ultrapure water (18.2
65 M Ω , ELGA Maxima) between each set of experiments to remove contaminants. Chamber RH,
66 measured to $\pm 2\%$ (Vaisala HMP234 HUMICAP), was increased in discrete steps up to
67 supersaturation by additions of high purity water vapor from a steel boiler.

68 Methylglyoxal solution samples (Alfa-Aesar) were pumped and stirred periodically to remove
69 as much water as possible. The resulting brown viscous liquid was heated to produce green
70 methylglyoxal gas (and a small, variable amount of water vapor) in a glass bulb at known
71 pressure. Bulb contents were then transferred into the chamber using dry N₂. Ammonium
72 sulfate (AS) and glycine seed aerosol particles were used as model particles for inorganic and
73 organic aerosol, respectively, since AS is a common aerosol salt species and glycine is the most
74 abundant amino acid in atmospheric aerosol.³²⁻³³ Both species are reactive towards

75 methylglyoxal.^{21, 34} Seed aerosol were produced by atomizing aqueous solutions of 1 – 2 mM
76 AS or 10 mM glycine. AS droplets were diffusion-dried before being sent into a dry chamber.
77 For glycine aerosol (Expt. 4), in order to generate a complex, atmospherically relevant surface
78 containing oligomers and more functional groups than just carboxylic acids and amines,
79 deliquesced glycine aerosol were “pre-reacted” with 1.0 ppm methylglyoxal and 0.68 ppm
80 methylamine at 72% RH for 90 minutes before methylglyoxal concentrations was increased to
81 6.9 ppm and its uptake measured. Aerosol and cloud droplet size distributions were respectively
82 monitored by SMPS (TSI 3080/3772, 20-900 nm, sampling via Nafion drying tube) and droplet
83 scattering spectrometer (Welas, Palas Particle Tech., 0.25 to 15 μ m, corrected for inlet losses³⁵).
84 Methylglyoxal gas concentrations in the chamber were calibrated using long-path FTIR (Bruker
85 Tensor, calibration Figure S1, integrated methylglyoxal band intensity = 6.3×10^{-18} cm²
86 molecule⁻¹ from 2720 to 2940 cm⁻¹)³⁶ and monitored by PTR-MS (KORE Tech. Series II)
87 through a 60 °C sampling line. Fast PTR-MS response to methylglyoxal additions (\leq 1 min.
88 chamber mixing time) indicated no significant partitioning of methylglyoxal to the sampling line.

89 The uptake coefficient γ is the fraction of collisions of a gas molecule with a surface that lead
90 to reactive uptake. The observed uptake coefficient, γ_{obs} , is calculated using eq. 1,

91
$$\gamma_{obs} = \frac{4k}{\bar{c} SA} \quad (1)$$

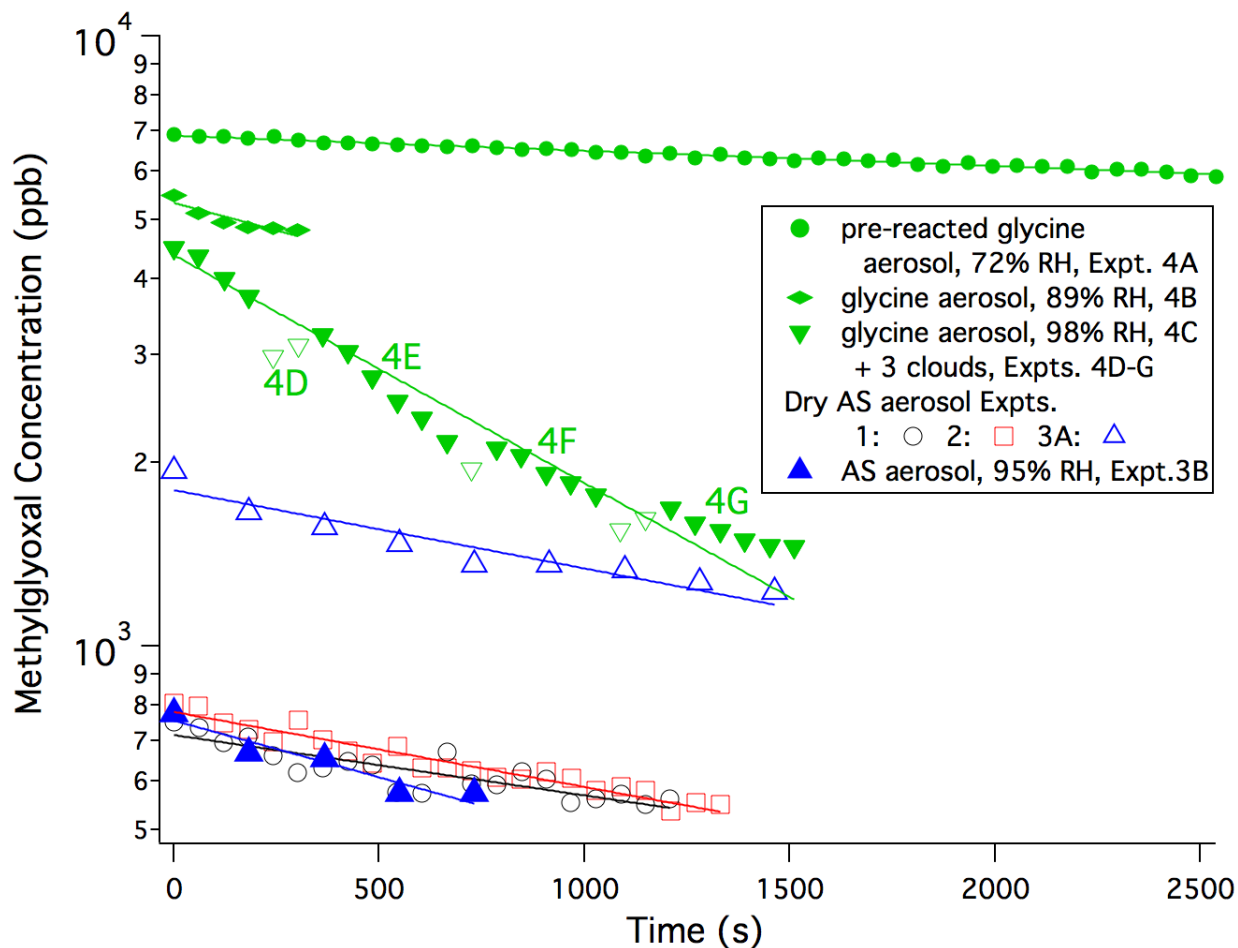
92 where k is the 1st-order rate constant (s⁻¹) extracted from the decay of gas-phase methylglyoxal
93 signals after RH-dependent wall losses were subtracted, SA is the SMPS-measured surface area
94 of aerosol (m² surface / m³ air) or other surface, and \bar{c} is the mean speed of methylglyoxal
95 molecules in m/s,

96
$$\bar{c} = \sqrt{\frac{8RT}{\pi M}} \quad (2)$$

97 where $R = 8.3145 \text{ J mol}^{-1}\text{K}^{-1}$, T is temperature (Kelvin), and M is the molecular mass of
98 methylglyoxal (0.072 kg/mol). Stated uncertainties in uptake coefficients include experimental
99 uncertainties in wall loss rates, aerosol surface areas, and 1st-order fits. The observed uptake
100 coefficient can be limited by gas-phase diffusion, mass accommodation, and/or reactivity and
101 diffusion in the condensed phase.³⁷ In this study, gas-phase diffusion was not the primary
102 limitation on observed uptake coefficients at $\text{RH} \leq 98\%$. At 99% RH, gas-phase diffusion
103 limitations likely suppressed the observed uptake coefficient by ~50%.

104 **3. Results**

105 Methylglyoxal concentrations measured by PTR-MS as a function of time in the chamber are
106 shown in Figure 1. Extracted first-order decay rate constants, aerosol or cloud surface areas, and
107 uptake coefficients are summarized in Table 1.



108

109 Figure 1: Methylglyoxal loss rates measured by PTR-MS, corrected for RH-dependent zero-
 110 order wall losses and sampling dilution in the constant-pressure CESAM chamber. Open
 111 symbols: dry chamber containing crystalline AS aerosol particles (black, Expt. 1; red, Expt. 2;
 112 blue, Expt. 3). Blue filled triangles (Expt. 3): chamber at $95 \pm 2\%$ RH containing deliquesced
 113 AS aerosol. Green circles, diamonds, triangles (Expt. 4): chamber at 72, 89, and $98 \pm 2\%$ RH,
 114 respectively, containing deliquesced, pre-reacted glycine aerosol (exposed to 1.0 ppm
 115 methylglyoxal and 0.68 ppm methylamine at 72% RH for 90 min. before methylglyoxal
 116 concentration was increased to 6.9 ppm for uptake measurements at 72% RH). Expts. 4A, 4B,
 117 and 4C were performed sequentially. Green open triangles show three brief drops
 118 corresponding to three cloud events with $RH > 100\%$; fit omits these data points. Expt 4C data
 119 is subdivided into labeled sections 4D (cloud 1) and 4E-4G (post-cloud 1-3, respectively).

120

121 **Table 1: Measured Methylglyoxal Uptake Rate Constants and Uptake Coefficients**

expt.	surface	% RH ($\pm 2\%$)	k_{surface} (10^{-4} s^{-1}) ^a	surface area ($10^{-3} \text{ m}^2/\text{m}^3$)	γ_{surface} (10^{-3})
1	AS	< 5	$< 2.3 \pm 0.3$	0.6^{b}	$< 4.6 \pm 0.6$
2	AS	< 5	$< 2.8 \pm 0.2$	0.7^{b}	$< 4.7 \pm 0.3$
3A	AS	< 5	$< 3.0 \pm 0.4$	1.0^{b}	$< 3.5 \pm 0.4$
3B	AS	95	4.3 ± 0.8	1.6^{b}	3.7 ± 0.8
4A	glycine	72	0.62 ± 0.08	2.3^{c}	0.37 ± 0.06
4B	glycine	89	4.2 ± 1.1	2.5^{c}	2.3 ± 0.6
4C	glycine	98	8.6 ± 0.9	4.2^{c}	2.8 ± 0.4
4D	cloud droplet	> 100	> 17	$80 - 500^{\text{c}}$	d
4E	cloud-processed glycine	~99	11.0 ± 1.1	2.3^{c}	6.6 ± 1.0
4F	cloud-reprocessed glycine	~99	6.9 ± 0.8	1.7^{c}	5.7 ± 0.9
4G	cloud-reprocessed glycine	~99	4.5 ± 0.8	1.3^{c}	4.8 ± 1.0

122 **a:** Data corrected using measured RH-dependent zero-order wall losses: $0.018 \pm 0.007 \text{ ppb s}^{-1}$
 123 at < 5% RH, $0.09 \pm 0.03 \text{ ppb s}^{-1}$ at 72% RH, and 0 ppb s^{-1} above 85% RH, where no net wall
 124 losses were observed due to equilibrium. **b:** SMPS aerosol particle surface area. **c:** WELAS
 125 aerosol particle surface area. **d:** Uptake not measurable because equilibrium achieved in <1 min.

126

127 **3.1 Wall losses.** Because the chamber has a surface area to volume ratio of $\sim 4.3 \text{ m}^2/\text{m}^3$,³⁰
 128 while aerosol in the chamber have $< 0.003 \text{ m}^2/\text{m}^3$ total surface area, it is critical that the uptake
 129 of methylglyoxal onto the steel chamber walls be well-characterized so that wall and aerosol
 130 surface processes can be distinguished. Fourteen methylglyoxal wall loss experiments were
 131 therefore conducted at various concentrations (35 ppb to 2.5 ppm) and RH levels (0 to 87%).
 132 Measured 1st-order wall loss rate constants are shown in Figure S2. Measured 1st order wall loss
 133 rate constants varied by a factor of 300 and showed a large, negative dependence on
 134 methylglyoxal concentrations. In other words, steel chamber walls appear to take up
 135 methylglyoxal at a nearly constant rate that is independent of methylglyoxal concentrations,

136 suggesting that under our experimental conditions methylglyoxal losses on the steel chamber
137 surfaces are limited by available surface uptake sites. In fact, we estimate that $\sim 6 \times 10^{19}$
138 methylglyoxal molecules, equivalent to 0.6 ppm in the CESAM chamber, would create a
139 monolayer if adsorbed on the steel chamber walls. This is near the concentration median of our
140 wall loss experiments, suggesting that competition for wall surface uptake sites could contribute
141 to the lower uptake rate constants observed in higher concentration runs.

142 The near-constant wall losses observed are better expressed as zero-order loss rates, shown as
143 a function of RH in Figure S3. Nine measurements at RH <15% were within a factor of 2 of
144 each other, with an average methylglyoxal loss rate of 0.018 ± 0.007 ppb s^{-1} . Five loss rate
145 measurements on two other days were higher by factors of 8.4 ± 0.5 and 33 (not shown in Figure
146 S3). In the latter case, chamber walls were known to be contaminated with ammonium sulfate
147 aerosol from earlier experiments. Thus, we take 0.018 ± 0.007 ppb s^{-1} as the loss rate of
148 methylglyoxal on clean and dry steel surfaces.

149 As relative humidity increases, the gas-phase reaction between methylglyoxal and water vapor
150 converts more methylglyoxal to its hydrated diol form.^{7, 9} Because the diol form of
151 methylglyoxal is less volatile, losses of methylglyoxal to surfaces are expected to increase, and
152 this is observed for wall losses in Figure S3 between 15 and 50% RH. However, at high RH,
153 enhanced uptake rates are offset by hydrolysis of wall-deposited methylglyoxal oligomers,²⁹
154 rapidly establishing a gas/surface equilibrium similar to that observed in glyoxal chamber
155 experiments.^{13, 15} For example, when the relative humidity was increased from 0 to $87 \pm 2\%$ in a
156 chamber experiment without seed particles, the gas-phase concentration of methylglyoxal
157 increased by a factor of 2.6 and reached equilibrium within 2 min, twice the chamber mixing
158 time. After this, methylglyoxal signals were quite stable over the next hour as the RH declined

159 from 87 to $82 \pm 2\%$, rising an additional $\sim 8\%$ (perhaps due to the contribution of a slow dimer
160 hydrolysis process).³⁸ Similar observations were made when the chamber contained wall-
161 deposited aerosol. We thus conclude that at $\text{RH} \geq 85\%$, methylglyoxal rapidly equilibrates with
162 the steel chamber walls, because no net wall uptake is observed beyond 2 min. Thus, no
163 correction for wall loss is made in methylglyoxal experiments at $\text{RH} \geq 85\%$, while between 15
164 and 85% RH (*i.e.*, for Expt. 4A only), we estimate wall loss corrections using a 3rd-order
165 polynomial fit to the wall loss measurements plotted vs. RH (Figure S3).

166 3.2 Dry AS aerosol (Expts 1 – 3A). Figure 1 shows loss rates measured by PTR-MS in 3
167 experiments after methylglyoxal was added to the dry chamber containing AS aerosol particles
168 (open symbols). After correcting the data for wall losses on clean and dry steel (0.018 ± 0.007
169 ppb s^{-1}), 1st order loss rate constants were calculated, and were found to increase with AS surface
170 areas, as expected (Table 1). The experiments show good consistency, with calculated uptake
171 coefficients $\gamma_{\text{AS,dry}}$ averaging $(4.3 \pm 0.) \times 10^{-3}$. This is an upper limit, however, because all 3
172 experiments were conducted with AS aerosol from previous experiments deposited on the walls,
173 and total observed loss rates were similar to maximum wall loss rates measured with wall-
174 deposited AS aerosol). Thus, wall-deposited AS aerosol may have contributed significantly to
175 observed methylglyoxal losses.

176 3.3 Deliquesced AS aerosol (Expt. 3B). Figure 1 also shows methylglyoxal uptake recorded
177 in the presence of AS aerosol immediately after the chamber RH increased from 79 to $95 \pm 2\%$
178 RH (filled blue triangles). This RH increase reached and exceeded the deliquescence point of the
179 previously dried AS aerosol, $80.6\% \text{ RH}$,³⁹ forming aqueous droplets. The loss rate of
180 methylglyoxal observed over the next 12 min by PTR-MS corresponds to a 1st-order rate
181 constant $k = (4.3 \pm 0.8) \times 10^{-4} \text{ s}^{-1}$. This loss rate could be due to increased methylglyoxal uptake

182 by the deliquesced aerosol particles or by the chamber walls at higher RH. However, 25 min
183 earlier, when the relative humidity of the seeded chamber was first increased to $79 \pm 2\%$, the
184 gas-phase methylglyoxal PTR-MS signals responded just as they did in the seed-free chamber:
185 methylglyoxal signals stabilized within 3 min after a fast initial rise, with only a slight
186 subsequent increase as RH levels dropped a few percent. This suggests that methylglyoxal
187 rapidly reached equilibrium with the humid walls long before the second RH increase from 79 to
188 $95 \pm 2\%$. While the methylglyoxal wall equilibrium may have been perturbed by the second RH
189 increase, unless this wall equilibrium takes much longer to establish itself at $95 \pm 2\%$ RH than at
190 79 or $87 \pm 2\%$ RH, it cannot explain the continuous 12-min decline observed in gas-phase
191 methylglyoxal signals. Methylglyoxal uptake onto newly deliquesced seed particles is a more
192 likely explanation of this signal decline.

193 The uptake coefficient from this methylglyoxal loss can be estimated given the uptake surface
194 areas. The AS aerosol size distribution in the $95 \pm 2\%$ RH chamber was measured after drying
195 to $62 \pm 4\%$ RH in the sampling line, due to a 7°C temperature differential between the cooled
196 chamber and the room temperature SMPS. This RH change should cause deliquesced AS
197 particles to shrink in diameter by a factor of 1.64 due to water loss.⁴⁰ The measured SMPS size
198 distribution at 62% RH was therefore multiplied by a growth factor of 1.64, resulting in an
199 estimated chamber aerosol surface area at $95 \pm 2\%$ RH of $1.58 \times 10^{-3} \text{ m}^2/\text{m}^3$. The methylglyoxal
200 uptake coefficient onto deliquesced AS aerosol is then $\gamma = (3.7 \pm 0.8) \times 10^{-3}$.

201 3.4 Deliquesced glycine aerosol (Expt. 4A - C). After deliquesced glycine aerosol, 0.68 ppm
202 methylamine, and 1.0 ppm methylglyoxal equilibrated in the chamber for 90 min. at $72 \pm 2\%$
203 RH, additional methylglyoxal was injected into the chamber to reach 6.9 ppm. Starting 10 min
204 later when PTR-MS data collection commenced, constant methylglyoxal losses were observed

205 for 40 min (Figure 1, Expt. 4A). The RH-dependent wall loss function shown in Figure S3 was
206 used to estimate the methylglyoxal wall loss rate at $72 \pm 2\%$ RH to be 0.09 ± 0.03 ppb s^{-1} , which
207 was $5\times$ lower than the observed total methylglyoxal loss rate, and resulted in a calculated first
208 order loss constant k of $(6.2 \pm 0.8) \times 10^{-5} s^{-1}$. The aerosol size distribution could be measured in
209 this experiment by both SMPS (dried) and droplet scattering spectrometer (wet). After these two
210 datasets were corrected for changes in RH during sampling and droplet losses in the inlet,
211 respectively, the surface areas measured by the two techniques agreed to within 16%. The
212 uptake coefficient is then $\gamma = (0.37 \pm 0.06) \times 10^{-3}$. We attribute this lower uptake to the fact that
213 the deliquesced glycine aerosol particles had already reacted with ≥ 1.0 ppm methylglyoxal and
214 0.68 ppm methylamine in the chamber for a total of 100 min. before the methylglyoxal uptake
215 rate was measured. At $72 \pm 2\%$ RH, the mole fraction of water in non-effloresced glycine
216 aerosol particles is 41%,⁴¹ and the water mass fraction is therefore only 14%. These meta-stable,
217 non-crystalline glycine seed particles may be quite viscous, such that surface “aging” is possible
218 and an aged surface may persist for hours.

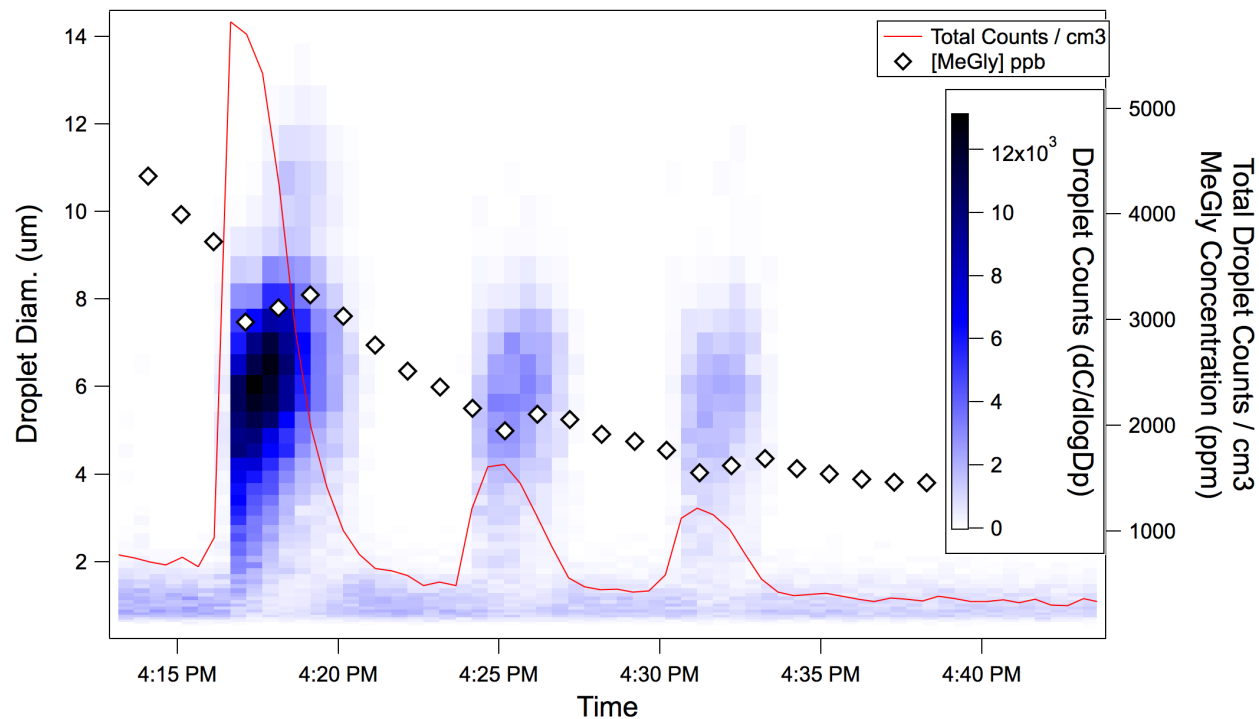
219 When the RH was increased to $89 \pm 2\%$, water content in the glycine seed aerosol should
220 increase to 22% by mass,⁴¹ reducing particle viscosity. This RH increase caused methylglyoxal
221 loss rates to increase more than 5-fold to $k = (4.2 \pm 1.1) \times 10^{-4} s^{-1}$ (Figure 1, Expt. 4B). No
222 change was observed in the methylamine gas concentration measured by PTR-MS or the surface
223 area of the fully dried aerosol measured by SMPS. Since methylamine concentrations did not
224 change, it is unlikely that methylglyoxal + methylamine reactions are the cause of the increased
225 methylglyoxal losses. The increase in methylglyoxal uptake rate is more likely due to increased
226 glycine aerosol surface area at higher RH. Surface area was estimated to be $(2.5 \pm 0.1) \times 10^{-3}$
227 m^2/m^3 using both hygroscopic growth corrected SMPS data and droplet spectrometer data

228 corrected for inlet losses (agreement to within 5%). The measured methylglyoxal uptake
229 corresponds to an uptake coefficient of $\gamma = (2.3 \pm 0.6) \times 10^{-3}$ for aqueous glycine aerosol at 89
230 $\pm 2\%$ RH.

231 When the RH was increased to near saturation ($98 \pm 2\%$ RH, Expt. 4C), the rate of
232 methylglyoxal losses more than doubled again to $k = (8.6 \pm 0.9) \times 10^{-4} \text{ s}^{-1}$. The effect of 3
233 intervening cloud events is discussed below, and cloud data points are omitted in the present
234 analysis. Near H_2O saturation, correcting SMPS measurements of dried aerosol with hygroscopic
235 growth factors introduces large uncertainties, so droplet spectrometer measurements of wet
236 particle surface area are more accurate. The addition of water vapor to increase RH from 89 to 98
237 $\pm 2\%$ caused an increase in wet aerosol surface area to $(4.2 \pm 0.4) \times 10^{-3} \text{ m}^2/\text{m}^3$, resulting in a
238 methylglyoxal uptake coefficient on aqueous glycine aerosol surfaces of $\gamma = (2.8 \pm 0.4) \times 10^{-3}$.
239 The similarity of this value to the uptake coefficient on aqueous AS aerosol at $95 \pm 2\%$ RH ($\gamma =$
240 $(3.7 \pm 0.8 \times 10^{-3})$) increases confidence in the analysis.

241 Figure 1 shows that the fit to methylglyoxal concentration data with cloud data points removed
242 is also a reasonable fit for the pre-cloud data (glycine aerosol at $98 \pm 2\%$ RH). In fact, if only the
243 four pre-cloud data points are used to calculate a methylglyoxal uptake coefficient, the result is
244 within 11% of the previously calculated uptake coefficient. However, it is also apparent from
245 Figure 1 that methylglyoxal loss rates decline after each cloud event. Fitting each of these slopes
246 separately and using the droplet spectrometer surface areas measured after each cloud event
247 allows estimates to be made of methylglyoxal uptake by “cloud-processed” glycine aerosol just
248 below the saturation point ($99 \pm 1\%$ RH). These estimates (Table 1, Expts. 4E – G) show that
249 methylglyoxal uptake rates decline with decreasing aerosol surface area, resulting in an average
250 uptake coefficient of $\gamma = (5.7 \pm 1.0) \times 10^{-3}$ for cloud-processed glycine at $99 \pm 1\%$ RH.

251 3.5 Cloud droplets (Expt. 4D). Figure 2 shows methylglyoxal PTR-MS signals and droplet
252 spectrometer size distributions and total droplet counts recorded during three cloud events in
253 Expt. 4. Each cloud event caused gas-phase methylglyoxal signals to decline initially, and then to
254 recover after a few minutes as the cloud dissipated, evidence of reversible uptake of
255 methylglyoxal by cloud droplets. These brief excursions in the methylglyoxal signals, which
256 occur at the rate of chamber mixing (~1 min), are superimposed on a longer-term loss trend that
257 we attribute to uptake on aqueous glycine aerosol particles and have already analyzed above.
258 The size of the brief decline caused by each cloud event is proportional to the peak cloud droplet
259 counts (Figure S4). Furthermore, because cloud droplet size distributions are initially similar,
260 methylglyoxal declines are also roughly proportional to peak cloud droplet surface areas. While
261 the 1-min time resolution of the data is clearly inadequate to follow this fast and reversible
262 process in detail, the first cloud event caused a 760 ppb drop in methylglyoxal concentrations
263 within 1 min, which would produce an in-cloud methylglyoxal concentration of 54 mM given the
264 maximum total cloud droplet volume of 2.5 mL for this cloud event. Since the gas phase
265 concentration after this uptake is 3.0 ppm, this corresponds to an effective Henry's law
266 coefficient of $1.8 \times 10^4 \text{ M atm}^{-1}$ at 27 °C, significantly above previously reported values ($3710 \pm$
267 320 M atm^{-1} at 25 °C).²⁴ This suggests that in these cloud events, the long-term declining trend
268 obscures the magnitude of the cloud effect, and that some of the observed methylglyoxal uptake
269 during cloud events is likely to the walls.) It appears that gas / cloud droplet equilibrium is
270 reached in < 1 min. for methylglyoxal, and uptake coefficients onto cloud surfaces can therefore
271 not be resolved by this experiment due to the slower (~1 min.) chamber mixing times.
272

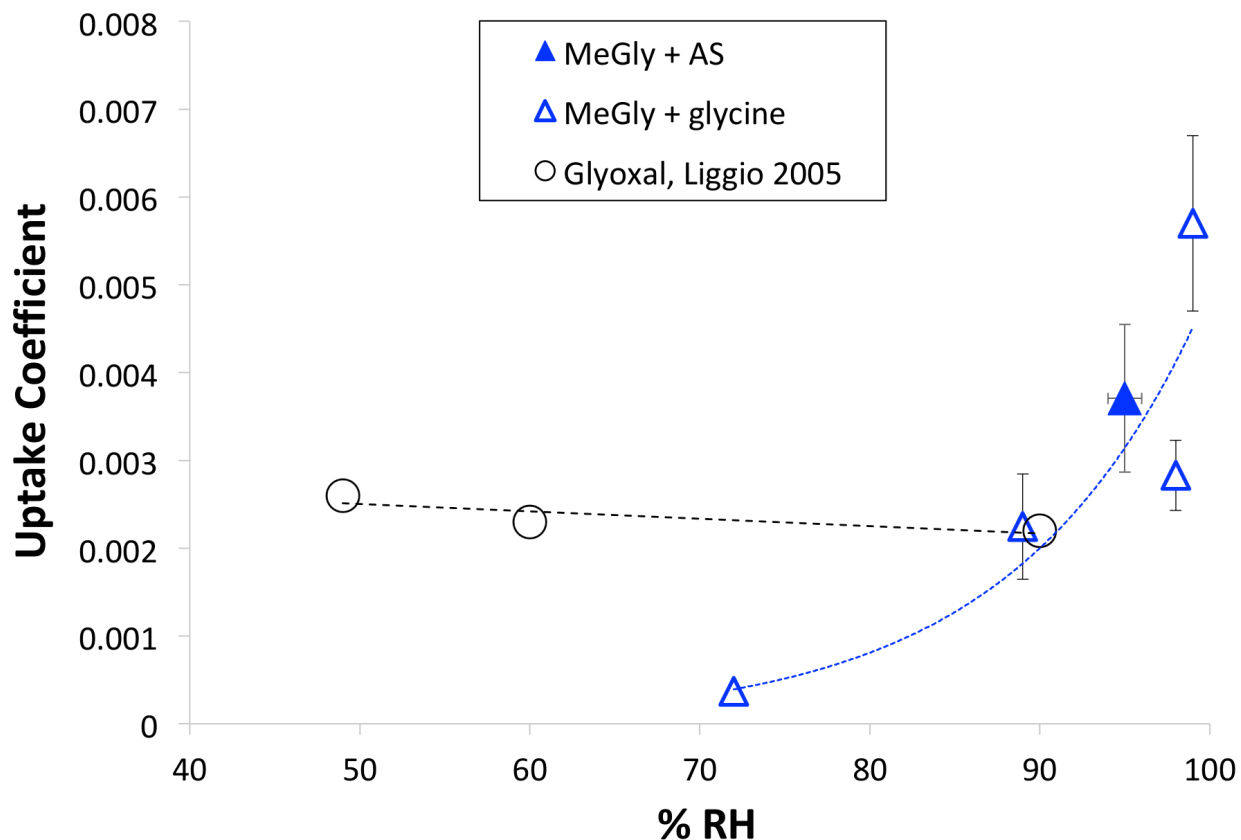


273
 274 Figure 2: Glycine aerosol activation and reversible uptake of methylglyoxal by 3 clouds (Expt.
 275 4). Blue color scale: cloud droplet spectra (30 s averaging, counts at each diameter size bin (left
 276 axis) vs. time). Red line: total droplet counts, corrected for inlet losses³⁵ (right axis). Open
 277 diamonds: PTR-MS methylglyoxal concentrations in ppb measured by PTR-MS (black
 278 diamonds, right axis).

279 4. Discussion

280 Figure 3 compares glyoxal uptake measurements on non-acidified (AS and sodium nitrate)
 281 aerosol surfaces reported by Liggió *et al.*¹³ with our methylglyoxal uptake measurements on
 282 aqueous AS and pre-reacted glycine seeds as a function of relative humidity. While glyoxal
 283 uptake to non-acidified aerosol does not appear to depend on RH, methylglyoxal uptake to pre-
 284 reacted glycine is strongly RH dependent, increasing by a factor of 15 between 72 and 99% RH.
 285 If we assume that glyoxal uptake coefficients are constant above 90% RH, in this range
 286 methylglyoxal uptake by aqueous aerosol surfaces is more efficient than glyoxal uptake. This is
 287 unexpected, since glyoxal has a higher effective Henry's law coefficient, especially in the
 288 presence of AS. The measured methylglyoxal uptake coefficient on cloud-processed glycine at

289 99% RH is also a factor of 2 larger than the $\gamma_{\text{glyoxal}} = 2.9 \times 10^{-3}$ value used for methylglyoxal
290 uptake to cloud droplets in some recent modeling studies.^{3, 17}



291
292 Figure 3: Comparison of measured uptake coefficients on non-acidified aerosol measured for
293 methylglyoxal (blue filled triangle, AS; blue open triangles, pre-reacted glycine aerosol) and
294 glyoxal (black open circles, AS and sodium nitrate aerosol, from ref¹³)

295 The observation from Figure 2 that uptake of methylglyoxal into cloud droplets is largely
296 reversible is consistent with droplet evaporation measurements, which showed that ~80% of the
297 methylglyoxal in a droplet consistently evaporated along with the water, even when ammonium
298 salts were present.⁴ Thus, treating methylglyoxal uptake to clouds as an irreversible process will
299 overestimate organic aerosol production by methylglyoxal in clouds by a factor of 5.

300 It is also important to note that the methylglyoxal PTRMS signals in Figure 2 recorded after
301 each cloud event are higher than would be predicted from extrapolation of the pre-cloud signals

302 in each case. This is especially obvious after the second cloud event at 4:25 pm. These post-
303 cloud increases in methylglyoxal gas concentrations indicate that cloud droplets do more than
304 take up methylglyoxal reversibly. The cloud droplets also appear to return to the gas phase a
305 fraction of the methylglyoxal that had previously been taken up by the aqueous glycine aerosol
306 particle that nucleated the droplet. The addition of abundant water to the aerosol particle upon
307 cloud nucleation likely hydrolyzes some methylglyoxal oligomers, adding to the monomer pool,
308 some of which dehydrate and return to the gas phase in order to reestablish equilibrium. This
309 hydrolytic loss of particle-phase methylglyoxal can evidently outpace hydration and deposition
310 of gas-phase methylglyoxal, even though the latter process is enhanced at high RH.^{7,9}

311 Fitting the methylglyoxal data before each cloud event and extrapolating to the first three after-
312 cloud measurements, we estimated the increase in methylglyoxal gas produced by each cloud
313 relative to the expectation from the previous trend, and compared these increases to the total
314 methylglyoxal taken up previously by aqueous glycine aerosol. The result is that cloud events 1
315 and 2 each returned 7.9 ± 1.2 % and cloud event 3 returned 3.4 ± 0.3 % of previously absorbed
316 aerosol-phase methylglyoxal back to the gas phase. In other words, approximately 20% of the
317 total aqueous methylglyoxal SOA produced in this experiment was hydrolyzed during cloud
318 processing back into methylglyoxal gas. Thus, even if methylglyoxal uptake appeared to be fully
319 irreversible based on an aerosol experiment, subsequent cloud processing can retroactively
320 change this conclusion.

321 Some reversibility in uptake of methylglyoxal to aqueous aerosol is also implied by the slight
322 curvature beyond the first-order fits that can be seen in Figure 1. While methylglyoxal uptake
323 onto glycine aerosol particles at 72 ± 2 % RH shows no visible curvature over 40 min, all data
324 collected with AS or glycine aerosol at $\text{RH} \geq 89$ % show some curvature. This may indicate that

325 methylglyoxal is being released from more diluted aqueous aerosol particles at rates that are
326 detectably increasing during the 15 – 25 min duration of these measurements.

327 **5. Conclusion**

328 Uptake coefficients of methylglyoxal onto aqueous glycine and AS aerosol particles were
329 found to be similar in magnitude, increasing with RH up to $(5.7 \pm 0.9) \times 10^{-3}$ at $99 \pm 1\%$ RH.
330 This maximum uptake coefficient is a factor of 2 larger than the one (borrowed from glyoxal
331 measurements) most commonly used in modeling studies of methylglyoxal uptake to clouds and
332 aqueous aerosol. In this work, methylglyoxal uptake during cloud events was rapid and
333 reversible, reaching equilibrium within the 1 min. mixing time of the chamber, and so precluding
334 calculation of uptake coefficients onto cloud droplets. Gas phase methylglyoxal concentrations
335 after cloud events were higher than predicted based on pre-cloud trends, indicating that each
336 cloud event caused the volatilization of 3 to 8% of aerosol phase methylglyoxal, likely via
337 oligomer hydrolysis. Finally, curvature in 1st-order plots of methylglyoxal losses to aqueous
338 aerosol particles at $\text{RH} \geq 89\%$ suggests that some methylglyoxal is being released from aqueous
339 aerosol to the gas phase. While equilibrium is not approached within 20 min., methylglyoxal
340 uptake to aqueous aerosol is at least partially reversible at $\text{RH} \geq 89\%$.

341 **Acknowledgments**

342 This work was supported by NSF grant AGS-1523178. The authors thank V. Vaida for
343 sharing critical methylglyoxal wall uptake data, R. Volkamer for helpful discussions, and
344 acknowledge CNRS-INSU for supporting CESAM as an open facility through the National
345 Instrument label. The CESAM chamber has received funding from the European Union's
346 Horizon 2020 research and innovation programme through the EUROCHAMP-2020
347 Infrastructure Activity under grant agreement No 730997.

348 **Supporting Information**

349 The Supporting Information is available free of charge on the ACS Publications website.

350 Methylglyoxal calibration data, methylglyoxal wall losses graphed against methylglyoxal
351 concentrations and relative humidity, and methylglyoxal losses during cloud events
352 graphed against peak cloud droplet counts.

353

354 **References**

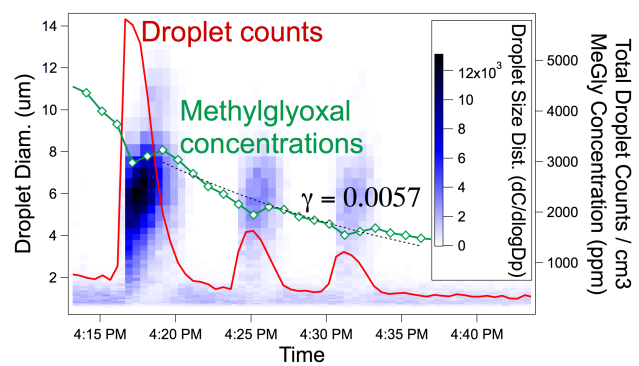
- 355 1. Stavrakou, T.; Müller, J.-F.; De Smedt, I.; Van Roozendael, M.; Kanakidou, M.; Vrekoussis,
356 M.; Wittrock, F.; Richter, A.; Burrows, J. P., The continental source of glyoxal estimated by
357 the synergistic use of spaceborne measurements and inverse modelling. *Atmos. Chem. Phys.*
358 **2009**, *9*, 8431-8446.
- 359 2. Myriokefalitakis, S.; Tsigaridis, K.; Mihalopoulos, N.; Sciare, J.; Nenes, A.; Kawamura, K.;
360 Segers, A.; Kanakidou, M., In-cloud oxalate formation in the global troposphere: a 3-D
361 modeling study. *Atmos. Chem. Phys.* **2011**, *11*, 5761-5782.
- 362 3. Fu, T.-M.; Jacob, D. J.; Wittrock, F.; Burrows, J. P.; Vrekoussis, M.; Henze, D. K., Global
363 budgets of atmospheric glyoxal and methylglyoxal, and implications for formation of
364 secondary organic aerosols. *J. Geophys. Res.* **2008**, *113*, D15303.
- 365 4. Galloway, M. M.; Powelson, M. H.; Sedehi, N.; Wood, S. E.; Millage, K. D.; Kononenko, J.
366 A.; Rynaski, A. D.; De Haan, D. O., Secondary organic aerosol formation during evaporation
367 of droplets containing atmospheric aldehydes, amines, and ammonium sulfate. *Environ Sci*
368 *Technol* **2014**, *48*, 14417-14425.
- 369 5. Ying, Q.; Cureño, I. V.; Chen, G.; Ali, S.; Zhang, H.; Malloy, M.; Bravo, H. A.; Sosa, R.,
370 Impacts of Stabilized Criegee Intermediates, surface uptake processes and higher aromatic
371 secondary organic aerosol yields on predicted PM_{2.5} concentrations in the Mexico City
372 Metropolitan Zone. *Atmos. Environ.* **2014**, *94*, 438-447.
- 373 6. Plath, K. L.; Axson, J. L.; Nelson, G. C.; Takahashi, K.; Skodje, R. T.; Vaidaa, V., Gas-phase
374 vibrational spectra of glyoxylic acid and its gem diol monohydrate. Implications for
375 atmospheric chemistry. *Reaction Kinetics and Catalysis Letters* **2009**, *96*, 209-224.
- 376 7. Axson, J. L.; Takahashi, K.; De Haan, D. O.; Vaida, V., Gas-phase water-mediated
377 equilibrium between methylglyoxal and its geminal diol. *P. Natl. Acad. Sci. USA* **2010**, *107*,
378 6687-6692.
- 379 8. Kumar, M.; Francisco, J. S., The Role of Catalysis in Alkanediol Decomposition:
380 Implications for General Detection of Alkanediols and Their Formation in the Atmosphere.
381 *The Journal of Physical Chemistry A* **2015**, *119*, 9821-9833.
- 382 9. Kroll, J. A.; Hansen, A. S.; Möller, K. H.; Axson, J. L.; Kjaergaard, H. G.; Vaida, V.,
383 Ultraviolet Spectroscopy of the Gas Phase Hydration of Methylglyoxal. *ACS Earth and*
384 *Space Chemistry* **2017**, *1*, 345-352.
- 385 10. Ervens, B.; Volkamer, R., Glyoxal processing by aerosol multiphase chemistry: towards a
386 kinetic modeling framework of secondary organic aerosol formation in aqueous particles.
387 *Atmos. Chem. Phys.* **2010**, *10*, 8219-8244.

- 388 11. Schweitzer, F.; Magi, L.; Mirabel, P.; George, C., Uptake rate measurements of
389 methanesulfonic acid and glyoxal by aqueous droplets. *J. Phys. Chem.* **1998**, *102*, 593-600.
- 390 12. Volkamer, R.; Ziemann, P. J.; Molina, M. J., Secondary organic aerosol formation from
391 acetylene (C₂H₂): seed effect on SOA yields due to organic photochemistry in the aerosol
392 aqueous phase. *Atmos. Chem. Phys.* **2009**, *9*, 1907-1928.
- 393 13. Liggio, J.; Li, S.-M.; McLaren, R., Reactive uptake of glyoxal by particulate matter. *J.*
394 *Geophys. Res.* **2005**, *110*, D10304.
- 395 14. Corrigan, A. L.; Hanley, S. W.; De Haan, D. O., Uptake of glyoxal by organic and inorganic
396 aerosol. *Environ. Sci. Technol.* **2008**, *42*, 4428-4433.
- 397 15. Kroll, J. H.; Ng, N. L.; Murphy, S. M.; Varutbangkul, V.; Flagan, R. C.; Seinfeld, J. H.,
398 Chamber studies of secondary organic aerosol growth by reactive uptake of simple carbonyl
399 compounds. *J. Geophys. Res.* **2005**, *110*, D23207.
- 400 16. Parikh, H. M.; Carlton, A. G.; Zhou, Y.; Zhang, H.; Kamens, R. M.; Vizuete, W., Modeling
401 secondary organic aerosol formation from xylene and aromatic mixtures using a dynamic
402 partitioning approach incorporating particle aqueous-phase chemistry (II). *Atmos. Environ.*
403 **2012**, *56*, 250-260.
- 404 17. Li, J.; Cleveland, M.; Ziemba, L. D.; Griffin, R. J.; Barsanti, K. C.; Pankow, J. F.; Ying, Q.,
405 Modeling regional secondary organic aerosol using the Master Chemical Mechanism. *Atmos.*
406 *Environ.* **2015**, *102*, 52-61.
- 407 18. Zhao, J.; Levitt, N. P.; Zhang, R.; Chen, J., Heterogeneous reactions of methylglyoxal in
408 acidic media: implications for secondary organic aerosol formation. *Environ. Sci. Technol.*
409 **2006**, *40*, 7682-7687.
- 410 19. Sareen, N.; Schwier, A. N.; Lathem, T. L.; Nenes, A.; McNeill, V. F., Surfactants from the
411 gas phase may promote cloud droplet formation. *Proc. Natl. Acad. Sci. (USA)* **2013**, *110*,
412 2723-2728.
- 413 20. Shapiro, E. L.; Szprengiel, J.; Sareen, N.; Jen, C. N.; Giordano, M. R.; McNeill, V. F., Light-
414 absorbing secondary organic material formed by glyoxal in aqueous aerosol mimics. *Atmos.*
415 *Chem. Phys.* **2009**, *9*, 2289-2300.
- 416 21. Sareen, N.; Schwier, A. N.; Shapiro, E. L.; Mitroo, D.; McNeill, V. F., Secondary organic
417 material formed by methylglyoxal in aqueous aerosol mimics. *Atmos. Chem. Phys.* **2010**, *10*,
418 997-1016.
- 419 22. Doussin, J. F.; Monod, A., Structure-activity relationship for the estimation of OH-oxidation
420 rate constants of carbonyl compounds in the aqueous phase. *Atmos. Chem. Phys.* **2013**, *13*,
421 11625-11641.
- 422 23. Raventos-Duran, T.; Camredon, M.; Valorso, R.; Mouchel-Vallon, C.; Aumont, B.,
423 Structure-activity relationships to estimate the effective Henry's law constants of organics of
424 atmospheric interest. *Atmos. Chem. Phys.* **2010**, *10*, 7643-7654.
- 425 24. Betterton, E. A.; Hoffmann, M. R., Henry's Law constants of some environmentally
426 important aldehydes. *Environ. Sci. Technol.* **1988**, *22*, 1415-1418.
- 427 25. Ip, H. S. S.; Huang, X. H. H.; Yu, J. Z., Effective Henry's law constants of glyoxal, glyoxylic
428 acid, and glycolic acid. *Geophys. Res. Lett.* **2009**, *36*, L01802.
- 429 26. Waxman, E. M.; Elm, J.; Kurtén, T.; Mikkelsen, K. V.; Ziemann, P. J.; Volkamer, R.,
430 Glyoxal and Methylglyoxal Setschenow Salting Constants in Sulfate, Nitrate, and Chloride
431 Solutions: Measurements and Gibbs Energies. *Environ Sci Technol* **2015**, *49*, 11500-11508.
- 432 27. Kua, J.; Hanley, S. W.; De Haan, D. O., Thermodynamics and kinetics of glyoxal dimer
433 formation: a computational study. *J. Phys. Chem.* **2008**, *112*, 66-72.

- 434 28. Krizner, H. E.; De Haan, D. O.; Kua, J., Thermodynamics and kinetics of methylglyoxal
435 dimer formation: A computational study. *J. Phys. Chem.* **2009**, *113*, 6994-7001.
- 436 29. De Haan, D. O.; Hawkins, L. N.; Welsh, H. G.; Pednekar, R.; Casar, J. R.; Pennington, E. A.;
437 de Loera, A.; Jimenez, N. G.; Symons, M. A.; Zauscher, M., *et al.*, Brown carbon production
438 in ammonium- or amine-containing aerosol particles by reactive uptake of methylglyoxal and
439 photolytic cloud cycling. *Environ Sci Technol* **2017**, *51*, 7458-7466.
- 440 30. Wang, J.; Doussin, J. F.; Perrier, S.; Perraudin, E.; Katrib, Y.; Pangui, E.; Picquet-Varrault,
441 B., Design of a new multi-phase experimental simulation chamber for atmospheric
442 photosmog, aerosol and cloud chemistry research. *Atmos. Meas. Tech.* **2011**, *4*, 2465-2494.
- 443 31. Denjean, C.; Formenti, P.; Picquet-Varrault, B.; Katrib, Y.; Pangui, E.; Zapf, P.; Doussin, J.
444 F., A new experimental approach to study the hygroscopic and optical properties of aerosols:
445 application to ammonium sulfate particles. *Atmos. Meas. Tech.* **2014**, *7*, 183-197.
- 446 32. Mopper, K.; Zika, R. G., Free amino acids in marine rains: evidence for oxidation and
447 potential role in nitrogen cycling. *Nature* **1987**, *325*, 246-249.
- 448 33. Zhang, Q.; Anastasio, C., Free and combined amino compounds in atmospheric fine particles
449 (PM_{2.5}) and fog waters from Northern California. *Atmos. Environ.* **2003**, *37*, 2247-2258.
- 450 34. De Haan, D. O.; Hawkins, L. N.; Kononenko, J. A.; Turley, J. J.; Corrigan, A. L.; Tolbert, M.
451 A.; Jimenez, J. L., Formation of nitrogen-containing oligomers by methylglyoxal and amines
452 in simulated evaporating cloud droplets. *Environ. Sci. Technol.* **2011**, *45*, 984-991.
- 453 35. von der Weiden, S.-L.; Drewnick, F.; Borrmann, S., Particle Loss Calculator — a new
454 software tool for the assessment of the performance of aerosol inlet systems. *Atmos. Meas.*
455 *Tech.* **2009**, *2*, 479-494.
- 456 36. Eurochamp, Eurochamp-2: Integration of European Simulation Chambers for Investigating
457 Atmospheric Processes. CEAM: Valencia, Spain, 2010.
- 458 37. Finlayson-Pitts, B. J.; Pitts, J. N., Jr., *Chemistry of the upper and lower atmosphere.*
459 Academic Press: San Diego, 2000.
- 460 38. Fratzke, A. R.; Reilly, P. J., Thermodynamic and kinetic analysis of the dimerization of
461 aqueous glyoxal. *Intl. J. Chem. Kinet.* **1986**, *18*, 775-789.
- 462 39. Zamora, I. R.; Tabazadeh, A.; Golden, D. M.; Jacobson, M. Z., Hygroscopic growth of
463 common organic aerosol solutes, including humic substances, as derived from water activity
464 measurements. *Journal of Geophysical Research: Atmospheres* **2011**, *116*, D23207
- 465 40. Topping, D. O.; McFiggans, G. B.; Coe, H., A curved multi-component aerosol
466 hygroscopicity model framework: Part 1 – Inorganic compounds. *Atmos. Chem. Phys.* **2005**,
467 *5*, 1205-1222.
- 468 41. Chan, M. N.; Choi, M. Y.; Ng, N. L.; Chan, C. K., Hygroscopicity of water-soluble organic
469 compounds in atmospheric aerosols: amino acids and biomass derived organic species.
470 *Environ. Sci. Technol.* **2005**, *39*, 1555-1562.

471

472 TOC artwork:



473

Supplemental Information:

Methylglyoxal Uptake Coefficients on Aqueous Aerosol Surfaces

David O. De Haan,^{1} Natalie G. Jimenez,¹ Alexia de Loera,¹ Mathieu Cazaunau,² Aline Gratien,² Edouard Pangui,² Jean-François Doussin²*

¹Department of Chemistry and Biochemistry, University of San Diego, 5998 Alcalá Park, San Diego CA 92110 USA

²Laboratoire Interuniversitaire des Systèmes Atmosphériques (LISA), UMR CNRS 7583, Université Paris-Est-Créteil (UPEC) et Université Paris Diderot (UPD), Institut Pierre Simon Laplace (IPSL), Créteil, France

Corresponding author contact: 011-1-619-260-6882, 011-1-619-260-2211 fax, ddehaan@sandiego.edu

5 pages (including cover sheet)

Figures S1 – S4

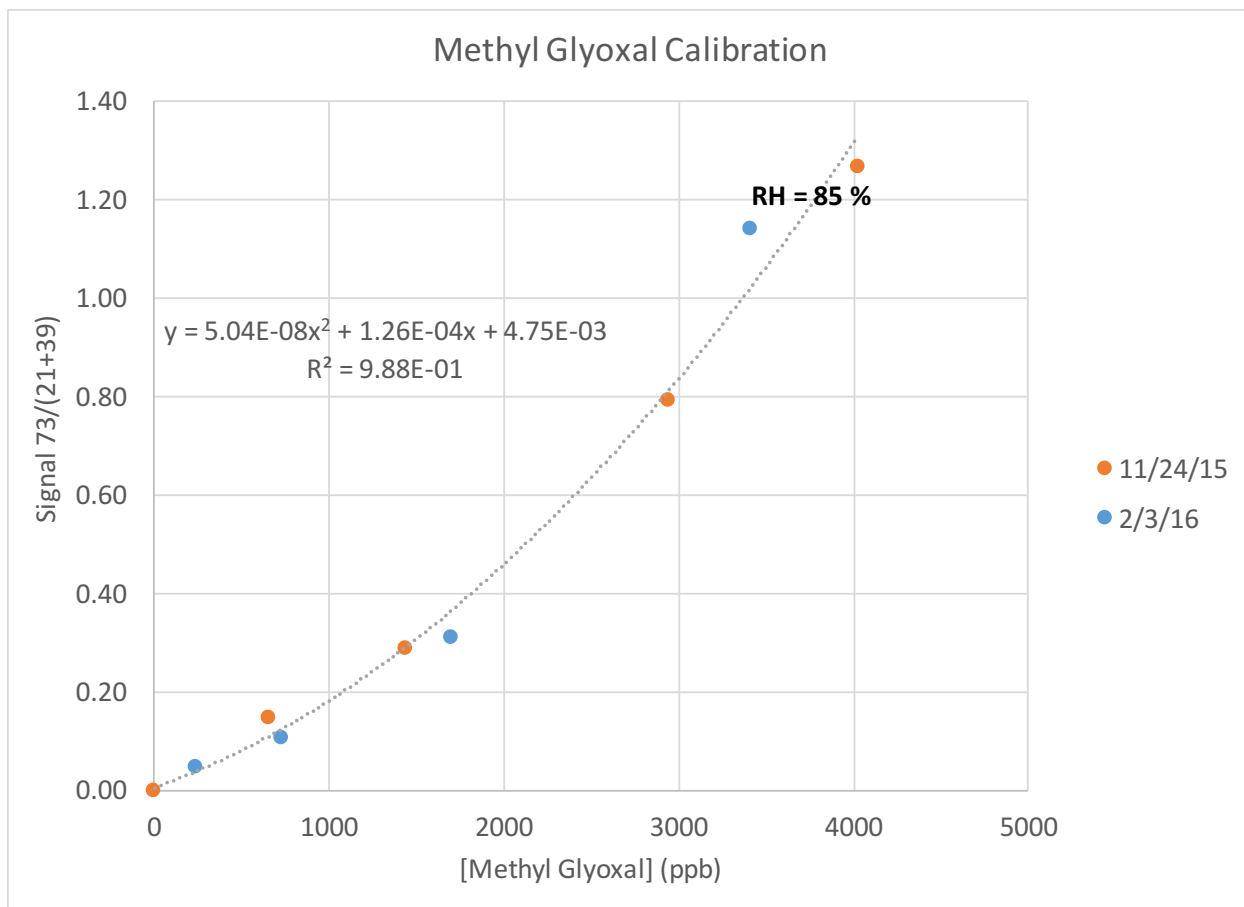


Figure S1: Calibration curve for water-corrected PTR-MS methylglyoxal signals vs concentrations in ppb based on FTIR absorbance bands.

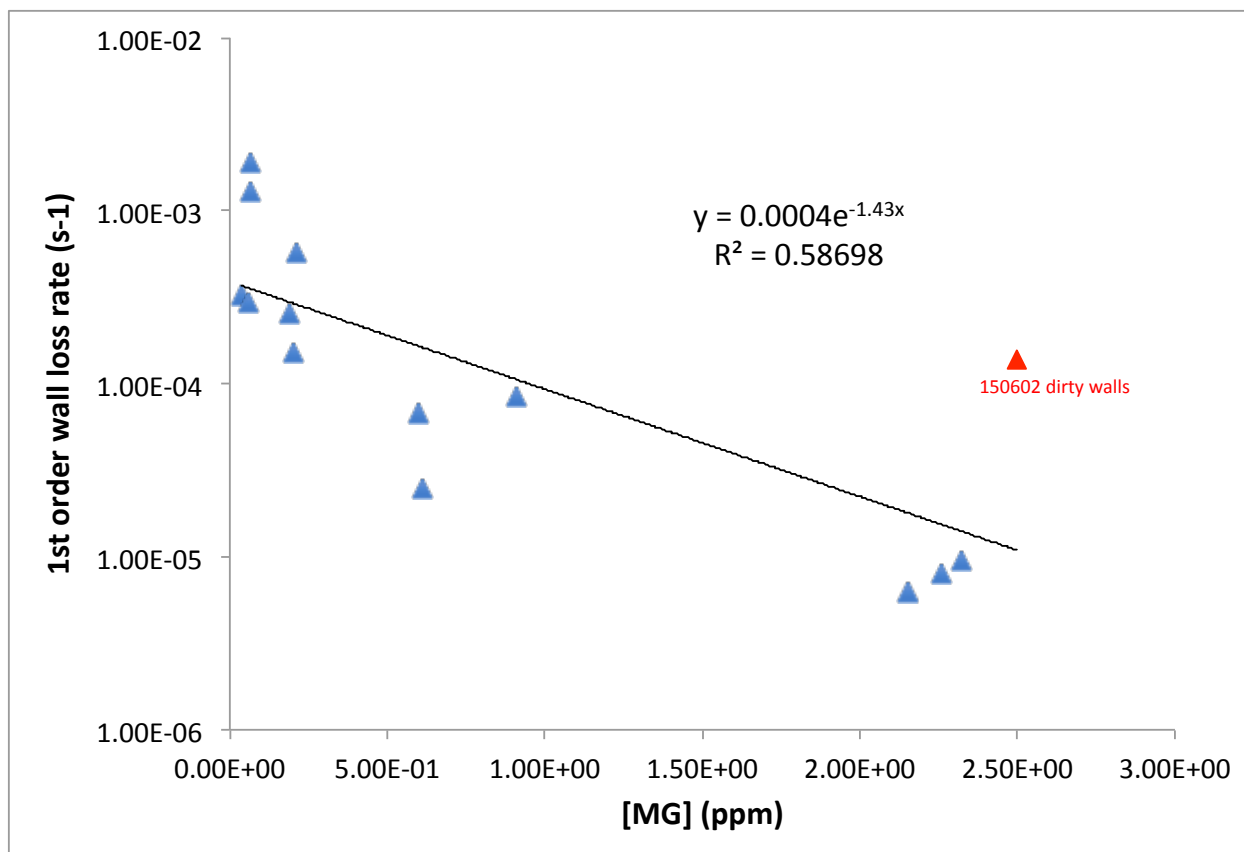


Figure S2: First order wall loss rates for methylglyoxal (s^{-1}) measured in dry ($RH \leq 15\%$), aerosol-free CESAM chamber as a function of methylglyoxal concentrations (ppm). First order wall loss rates varied by a factor of 300 and showed a dependence on [MeGly]. Red triangle denotes run where methylglyoxal wall uptake was measured in chamber that had been used for ammonium sulfate aerosol experiments for the previous week, such that wall uptake was likely enhanced by previously deposited AS aerosol. Other wall loss measurement runs (blue triangles) did not have significant quantities of aerosol particles deposited on the chamber walls.

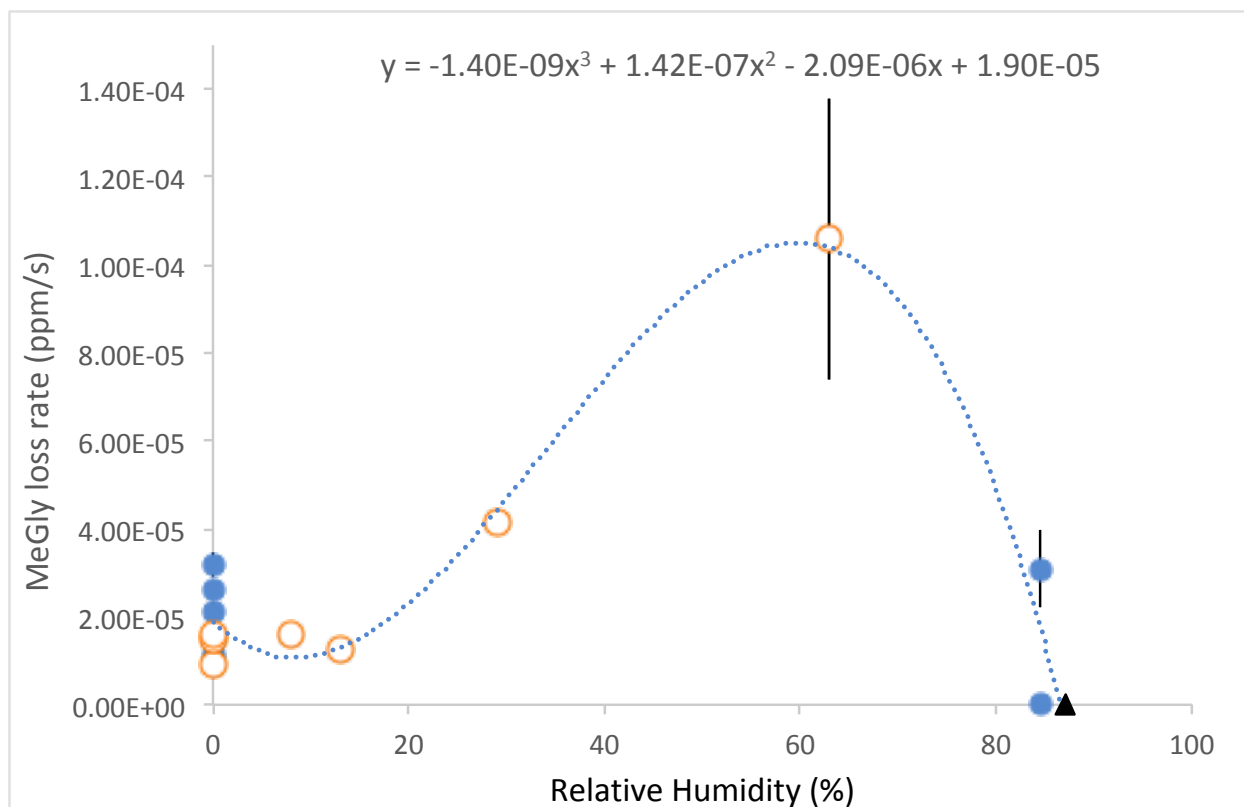


Figure S3: Zero order wall loss rates for methylglyoxal (in ppm s⁻¹) measured in aerosol-free CESAM chamber as a function of relative humidity. Different symbols denote data measured on different days. No data from experiments with wall-deposited aerosol is included.

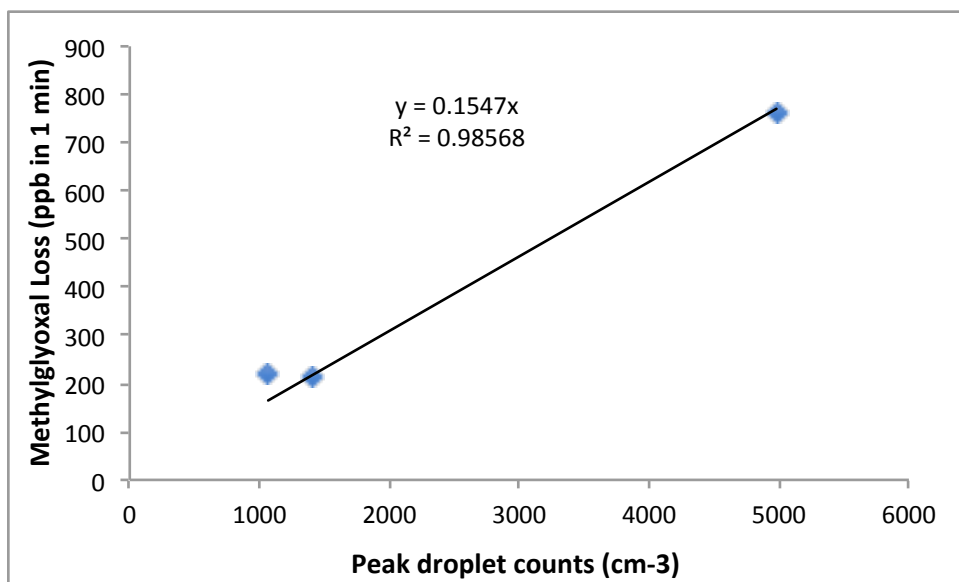


Figure S4: Methylglyoxal losses (in ppb) recorded by PTR-MS over 1 minute time step during three cloud events, graphed as a function of peak droplet counts recorded by droplet spectrometer. Pre-reacted glycine seed aerosol served as cloud condensation nuclei.